

BASIN-SCALE ASSESSMENT OF GAS HYDRATE DISSOCIATION IN RESPONSE TO CLIMATE CHANGE

**Matthew T. Reagan,
George J. Moridis
Earth Sciences Division
Lawrence Berkeley National Laboratory
Berkeley, CA 94720
UNITED STATES**

**Scott M. Elliott,
Mathew Maltrud
Los Alamos National Laboratory
Los Alamos, NM 87545
UNITED STATES**

**Philip J. Cameron-Smith
Lawrence Livermore National Laboratory
Livermore, CA 94550
UNITED STATES**

ABSTRACT

Paleoceanographic evidence has been used to postulate that methane from oceanic hydrates may have had a significant role in regulating climate. However, the behavior of contemporary oceanic methane hydrate deposits subjected to rapid temperature changes, like those now occurring in the arctic and those predicted under future climate change scenarios, has only recently been investigated. Field investigations have discovered substantial methane gas plumes exiting the seafloor along the Arctic Ocean margin, and the plumes appear at depths corresponding to the upper limit of a receding gas hydrate stability zone. It has been suggested that these plumes may be the first visible signs of the dissociation of shallow hydrate deposits due to ongoing climate change in the arctic. We simulate the release of methane from oceanic deposits, including the effects of fully-coupled heat transfer, fluid flow, hydrate dissociation, and other thermodynamic processes, for systems representative of segments of the Arctic Ocean margins. The modeling encompasses a range of shallow hydrate deposits from the landward limit of the hydrate stability zone down to water depths beyond the expected range of century-scale temperature changes. We impose temperature changes corresponding to predicted rates of climate change-related ocean warming and examine the possibility of hydrate dissociation and the release of methane. The assessment is performed at local-, regional-, and basin-scales. The simulation results are consistent with the hypothesis that dissociating shallow hydrates alone can result in significant methane fluxes at the seafloor. However, the methane release is likely to be confined to a narrow region of high dissociation susceptibility, defined by depth and temperature, and that any release will be continuous and controlled, rather than explosive. This modeling also establishes the first realistic bounds for methane release along the arctic continental shelf for potential hydrate dissociation scenarios, and ongoing work may help confirm whether climate change is already impacting the stability of the vast oceanic hydrate reservoir.

Keywords: gas hydrates, climate change

NOMENCLATURE

T , Temperature ($^{\circ}\text{C}$)
 P , Pressure (MPa)
 t , Time (yr)
 z , Distance below seafloor (m)
 k , Intrinsic permeability (m^2 , mD)
 k_s , Thermal conductivity (W/m-K)
 Φ , Porosity
 S , Phase saturation
 Q , Seafloor methane flux (mol/yr/m^2 ; mol/yr)
 V , Cumulative methane flux (mol/m^2 ; mol)
 X , Aqueous salt concentration

INTRODUCTION

Gas hydrates are solid crystalline compounds in which gas molecules are lodged within the lattices of water clathrate crystals [1]. Natural gas hydrate deposits occur in geologic settings where the necessary low temperatures and high pressures exist for their formation and stability--in the permafrost and in deep ocean sediments. The existing literature indicates that the global methane hydrate reserves are enormous. These estimates began with an initial "consensus value" of 10,000 Gt through work by various investigators [2,3,4]. More recently, Milkov [5] proposed a total of 500-2,500 Gt of methane-derived carbon, but two of the most recent studies have produced a wider range, from an upper estimate of 74,400 Gt of methane carbon in hydrate form [6] (27,300 Gt along continental margins) a lower estimate of 3,000 Gt of methane in hydrate and 2,000 Gt of gaseous methane existing in a stable state under current climate conditions [7].

In oceanic deposits, the range of depth over which hydrates remain stable (the gas hydrate stability zone, GHSZ) depends on the pressure P (imposed by the water depth) and temperature T . The landward limit of the GHSZ may extend upward to 300 m - 400 m depths when water temperatures are sufficiently cold. An increase in ocean water temperature at the seafloor above a shallow hydrate deposit lowers the top of the GHSZ (quickly) and raises the bottom of the GHSZ (after sufficient time has elapsed for heat to penetrate the deposit). The subsurface temperature profile now intersects a reduced region of the hydrate stability curve (as defined by depth/pressure) and hydrate is destabilized and may dissociate. This process of hydrate dissociation is regulated by multiple

factors, including flow of heat from below the hydrate deposit, fluid flow induced by hydrate dissociation, the thermal properties of the sediments, and the enthalpy of dissociation of the hydrates themselves [8]. Shallow deposits are more prone to destabilization due to their proximity to the landward edge of the GHSZ [8,9]. Hundreds of Gt of methane are expected to exist within Arctic Ocean sediments, [7] and recent observations have lead to a hypothesis that methane release due to hydrate dissociation may already be occurring [10,11]. Such releases, if widespread, could have potentially severe climatic and ecological consequences, in a scenario known as the "Clathrate Gun" [12].

The Clathrate Gun hypothesis has been challenged by different interpretations of the paleoclimatic data, estimations of actual hydrate extent, and simulations modeling hydrate stability. Deep (>1000m) hydrates may be relatively insensitive to ocean temperature shifts on short time scales [9,13]. Kvenvolden [3] and others have suggested that methane from dissociating hydrates may never reach the atmosphere, oxidizing to carbon dioxide in the water column [14]. A recent set of coupled methane release/methane oxidation/ocean transport simulations [15,16] suggest that resource limitations, including available oxygen, available nutrients, and the rate of ventilation of the ocean basin may hinder this mitigation, and that reductions in dissolved oxygen may be an unexpected negative by-product. Recent studies of the aftermath of the Macondo well blowout (which injected a large quantity of methane into Gulf waters) suggest this may be a possible outcome of large-scale methane release [17].

As no conclusive evidence has been put forth to confirm or discount the possible importance of hydrate-derived methane in climate cycles, a careful assessment is required. This paper describes part of a multi-year study to carefully and quantitatively study the potential for hydrate-derived methane release and estimate the possible ecological and atmospheric consequences.

MODELS AND METHODS

Simulation tools. The TOUGH+HYDRATE code [18] used in this study describes multiphase flow

and transport in hydrate-bearing geologic media. It includes coupled mass and energy transport within porous and/or fractured media, and also describes the full phase behavior of water, methane, solid hydrate, ice, and inhibitor species. The TOUGH+HYDRATE code has been used to (a) design the first field test of gas production from hydrate deposits in the Mallik area, Mackenzie Delta, Northwest Territories, Canada [19], (b) to analyze the results of the field study and determine the values of important parameters, (c) to evaluate the gas production potential of hydrates from both permafrost and ocean accumulations [20,21] and (d) to investigate the effects of hydrate dissociation on the geomechanical stability of hydrate-bearing sediments [22]. This code, also validated in laboratory experiments [23], was used in previous studies of hydrate dissociation in oceanic sediments [8,9,11]. This work is a continuation and expansion of that research.

Parameter	Value
Initial salt mass fraction in the ocean and pore water X_0	0.035
Gas composition	100% CH ₄
Base permeability k	$10^{-15} \text{ m}^2 (= 1 \text{ mD})$
Porosity ϕ	0.50
Dry thermal conductivity k_{sd}	1.0 W/m/K
Wet thermal conductivity k_{sw}	3.1 W/m/K
Composite thermal conductivity k_c : [32]	$k_{\Theta} = (\sqrt{S_H} + \sqrt{S_A}) (k_{sw} - k_{sd}) + k_{sd}$
Capillary pressure model, Van Genuchten [33]	$P_{cap} = -P_0 \left[(S^*)^{-1/\lambda} - 1 \right]^{-\lambda}$ $S^* = \frac{(S_A - S_{irA})}{(S_{mxA} - S_{irA})}$
P_0	2000 Pa
λ	0.45
Relative permeability model: Modified Stone [34]	$k_{rA} = (S_A^*)^n$ $k_{rG} = (S_G^*)^n$ $S_A^* = (S_A - S_{irA}) / (1 - S_{irA})$ $S_G^* = (S_G - S_{irG}) / (1 - S_{irA})$
n	4
S_{irG}	0.02
S_{irA}	0.20

Table 1. Physical properties parameters for the hydrate-bearing sediment system.

Setup of 1-D system. We simulate disperse, low-saturation deposits with an initial hydrate saturation, S_{H0} , of 0.03 reflecting the high end of

the estimated global average saturation for stratigraphic deposits. We simulate temperature and pressure conditions representing the Beaufort Sea continental shelf from a depth of $z = -300 \text{ m}$, above the top of the likely GHSZ for non-permafrost-associated hydrates, to $z = -1000 \text{ m}$, a depth at which any hydrates, if present, are expected to not show sensitivity to temperature changes and where short-term temperature changes are expected to be less pronounced. Initial seafloor temperatures range from $T_0 = 0.5 \text{ } ^\circ\text{C} - 1 \text{ } ^\circ\text{C}$, varying with depth, and we assume a geothermal gradient of $3 \text{ } ^\circ\text{C} / 100\text{m}$.

The representation of each depth/location involves a vertical, 1-D domain describing the sediment column from the seafloor down to $z = -360 \text{ m}$, well below the expected range of century-scale temperature perturbations. The initial condition is uniform S_H in the sediment column from the seafloor to the bottom of the GHSZ, and a system at complete thermal, chemical, and hydrostatic equilibrium, establishing hydrate distributions, saturations, and aqueous methane concentrations that correspond to the conditions at the selected depth and temperature. These deposits are assumed to be at steady state before any temperature changes occur, and are not connected to active seeps or methane sources, and as such these simulations only include methane derived from hydrate dissociation.

Physical parameters for the sediments are listed in Table 1. The intrinsic permeability, $k = 10^{-15} \text{ m}^2$ (1.0 mD), is within the reported range of oceanic sediments [26,27] and represents the more common stratigraphic deposits [5,24], in contrast to the less common, more permeable, and often more saturated structural deposits near sites of active methane seepage and/or venting. The porosity $\Phi = 0.5$ is typical for unconsolidated marine sediments and reflects core data from well-studied areas of suspected hydrate dissociation in an arctic environment [28,29]. The top of the sediment column is an open boundary, allowing heat and mass transfer between the sediment and the ocean.

Results from global climate simulations coupling ocean circulation, atmospheric circulation, and atmospheric chemistry [30] suggest that, under current climate conditions and a 1%/yr increase in atmospheric CO₂ concentration, the temperature at

the seafloor would rise by 1 °C or more over the next 100 yr, and possibly by another 3 °C in the following century. The actual degree of warming and the time-temperature profiles vary greatly with location and model parameters (Figure 1), with the Arctic continental shelf experiencing warming of approximately 3 °C/100 yr off the north slope of Alaska, but as much as 6 °C/100 yr of warming in regions affected by northward-flowing ocean currents, such as the Barents Sea or the Bering Sea shelf.

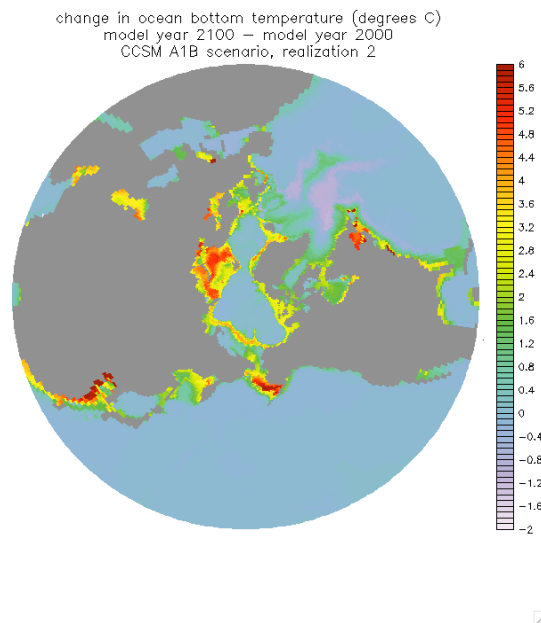


Figure 1. Anticipated ocean warming at the seafloor, for the IPCC A1B scenario for the years 2000-2100.

To capture a range of processes, we restrict our representation of ocean warming to simple linear temperature increases of $\Delta T = 1, 3, 5$, and 7 °C over a 100 yr period to describe the evolution of ocean temperature at the seafloor. Constant pressure (corresponding to a constant ocean water depth and salinity) is maintained at the top of the sediment column, while the temperature at the top boundary (corresponding to the water at the ocean floor), is varied. We record methane fluxes and fluid flow velocities at the seafloor, as well as the pressure, temperature, and phase saturation profiles at regular intervals. After 100 yr, the temperature is held constant (as predicting temperature changes beyond this point becomes increasingly speculative), and the system is allowed to evolve toward a new equilibrium for up to $t = 1,000$ yr. We perform these simulations at

regular depth intervals from 300 m down to 1,000 m to assess point-by-point potential for release across a wide range of the Arctic shelf. These simulations, although rough schematics of the wide range of possible hydrate depths, distributions, and saturations, allow a systematic examination of the many coupled processes that drive and regulate possible hydrate dissociation.

RESULTS

The simulations performed as part of this basin-scale study cover a wide range of depth, temperature, and ΔT . To illustrate the process of dissociation, we present a select group of the most relevant results at regular intervals. For Arctic conditions, 300 m water depth is insufficient to create a GHSZ at thermal equilibrium, and systems in more than 700 m of water produce extremely small methane fluxes for the temperature changes studied here [see also, 8]. Therefore, we focus on water depths that are in the most temperature sensitive zone: 350 m, 400 m, 450 m, 500 m, 550 m, 600 m, and 700 m.

Process of dissociation. Figures 2 and 3 illustrate the process of top-down dissociation seen for cold, shallow hydrate systems subjected to warming on timescales of 100 yr. In Figure 2, we see three 1-D snapshots of the dissociation process for a hydrate system located in 350 m water and subjected to a linear $+3$ °C temperature change at the seafloor over 100 yr. At $t = 10$ yr, the temperature profile (red line), shows a $+0.3$ °C perturbation at the seafloor ($z = 0$ mbsf), and that this temperature change has propagated only a few meters into the sediments, leaving the hydrates (green line, S_H) unaffected and generating no free gas (blue line, S_G). By $t = 50$ yr, however, the temperature change has propagated tens of meters, with the upper 20 m of the deposit exhibiting an inverted geothermal gradient. The upper 20 m of the column is now hydrate-free, and the methane gas saturation, S_G , has reached 11%. This free gas is mobile and buoyant, and may exit the sediment column through the upper boundary, along with any dissolved methane present in the mobile pore water that is driven out of the system through the expansion of gas from dissociation. At $t = 100$ yr, the temperature at the seafloor has increased to 4 °C, this change has propagated deep into the sediment column, dissociation has progressed such that the upper 42 m of the sediment column is hydrate-free, S_G approaches 11%, and an inverted

temperature gradient exists down to the dissociation boundary. Note the sharp turn in the temperature profile at $z = -42$ m. As the hydrate dissociation process is endothermic, we see the formation of a sharp dissociation front and an “orderly” top-down dissociation process. As noted in previous papers [8,9], this discounts the notion of “explosive” hydrate dissociation due to ocean warming. Only a system with impermeable but geomechanically weak confining boundaries is likely to exhibit explosive release, and then only if the dissociation has time to proceed and create a gas-rich, overpressured system.

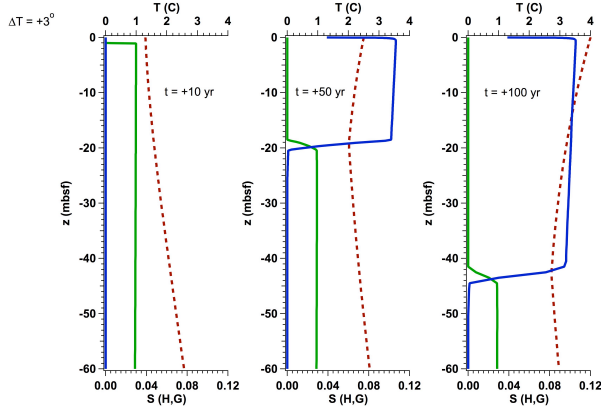


Figure 2. Dissociation of a hydrate system at 350 m depth, subjected to $+3$ °C/100 yr warming, at $t = 10, 50$, and 100 yr after the initiation of seafloor warming. The green line represents hydrate saturation, S_H , the blue line gas saturation, S_G , and the red line the temperature profile.

Figure 3 illustrates the variation of the dissociation process with deposit depth (with the indicated depth representing the depth of water above the overlying seafloor), through comparison of 1-D snapshots at $t = 100$ yr for systems at 350 m, 450 m, and 500 m water depth. In the second panel of Figure 3, we see that a deposit subjected to the same warming ($+3$ °C) over the same time period but existing at 100 m greater depth has progressed far less along the dissociation pathway than one at 350 m depth. Only approximately ~ 1 m of hydrate has dissociated at $t = 100$ yr, creating only a small region of free gas. However, the temperature change has propagated a significant distance into the formation, with an inverted T -gradient existing to a depth of -45 mbsf. The greater depth of the deposit results in a higher initial pressure and increased hydrate stability. In the third panel of Figure 3, we see that a deposit 50 m deeper, in 500

m of water, shows no sign of dissociation at $t = 100$ yr, despite that the temperature change has again propagated a significant distance into the sediments. These illustrations suggest that hydrate dissociation may be limited to a narrow range of deposit depths and temperatures.

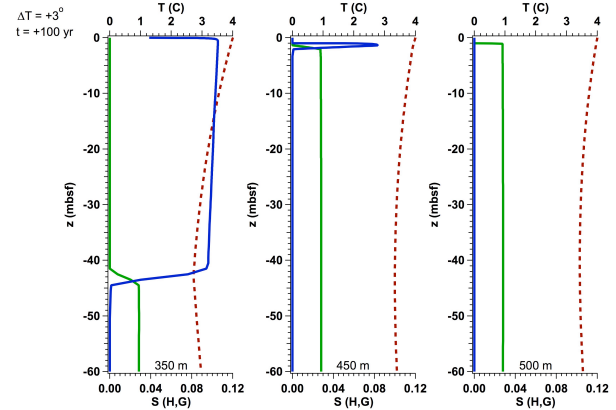


Figure 3. Dissociation of hydrate systems at 350 m, 450 m, and 500 m depth, subjected to $+3$ °C/100 yr warming, at $t = 100$ yr after the initiation of seafloor warming. The green line represents hydrate saturation, S_H , the blue line gas saturation, S_G , and the red line the temperature profile.

Evolution of fluxes. The evolution of instantaneous methane flux at the seafloor vs. time can be seen in Figure 4. For a deposit in 350 m of overlying water (solid lines), the flux, Q_{CH_4} , ranges from a maximum of 14.0 mol/yr/m² for a ΔT of $+7$ °C/100 yr to 7.6 mol/yr/m² for $\Delta T = +1$ °C/100 yr. Warming a deeper system, in 450 m of water, results in considerably lower fluxes (dotted lines). In this case, the maximum Q_{CH_4} of 5.6 mol/yr/m² occurs at $\Delta T = +7$ °C/100 yr, while for a ΔT of $+1$ °C/100 yr, $Q_{CH_4} < 0.2$ mol/yr/m². For an even deeper case, 600 m (dashed lines), even a temperature change of $+7$ °C/100 yr (at or above the upper limit of expected arctic warming scenarios), produces only $Q_{CH_4} \sim 0.2$ mol/yr/m², and this magnitude of methane release does not occur until the third century after the onset of warming. This is consistent with the notable depth-sensitivity of hydrate stability and agrees with previous work showing that the vast majority of deep stratigraphic hydrates are unlikely to experience large-scale dissociation due to any expected warming scenario.

Evolution of cumulative methane release. To better capture the consequences of methane

release, cumulative fluxes of methane vs. time better illustrate the input to the ocean for a given warming/dissociation scenario. Figures 5 and 6 illustrate the potential cumulative fluxes of methane, V_{CH_4} , into the ocean for various depth/temperature scenarios.

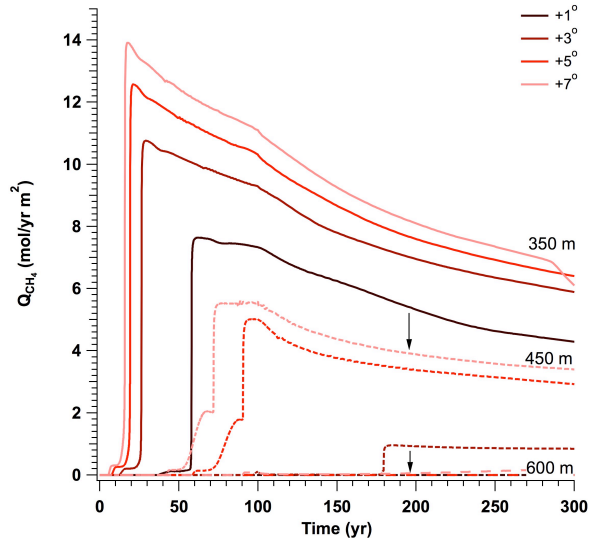


Figure 4. Local fluxes of methane in gaseous and aqueous phases for $\Delta T = +1, +3, +5$, and $+7^\circ \text{C}/100 \text{ yr}$ at the seafloor, for deposits where the seafloor is at 350 m, 450 m, and 500 m depth. The 350 m cases are represented by solid lines, the 450 m cases by dotted lines, and the 600 m cases by dashed lines.

In Figure 5, the cumulative methane flux, V_{CH_4} , for a range of water depths is presented for two temperature scenarios (note the log scale for V_{CH_4}). For a case of more significant warming, $\Delta T = +5^\circ \text{C}/100 \text{ yr}$ (top), the cumulative methane released in aqueous and gaseous forms at 350 m water depth approaches 1000 mol/m^2 at the end of the first century of warming, and then methane release continues to evolve, reaching nearly 2500 mol/m^2 by the end of 300 yr. At 400 m, V_{CH_4} approaches 1000 mol/m^2 after 300 yr, and at 450 m, 600 mol/m^2 at the same point in time. Cumulative fluxes decline significantly with depth, however, dropping to $V_{CH_4} = 330 \text{ mol/m}^2$ at 500 m and to only 4.6 mol/m^2 for systems in 550 m of water. Below 550 m, the amount of methane released is far less significant.

Two effects are in play here—1) increasing water depth results in increased initial pressure, such that a higher temperature is required to destabilize the

hydrate and 2) deeper systems have a slightly colder initial temperature (ranging from approximately 1.0°C at 350 m - 400 m depth to 0.5°C below 550 m for the case of the Beaufort shelf).

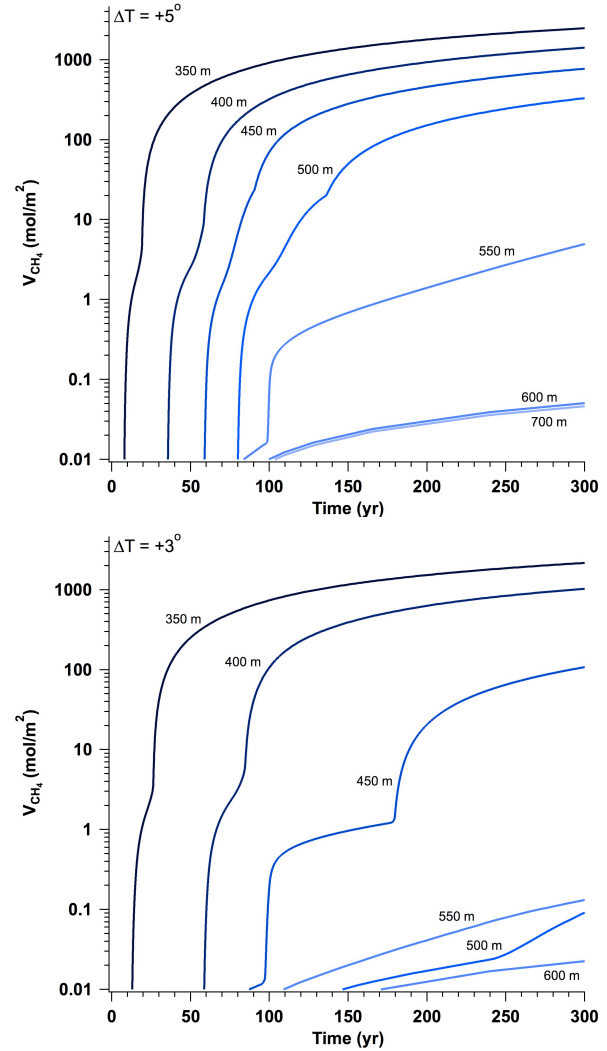


Figure 5. Cumulative local fluxes of methane in gaseous and aqueous phases, V_{CH_4} , at the seafloor for deposits where the seafloor is at 350 m to 700 m depth, for $\Delta T = +5^\circ \text{C}$ (top) and $+3^\circ \text{C}/100 \text{ yr}$ (bottom). Note the log scale for V_{CH_4} .

As a result, although the propagation of the temperature change proceeds at roughly the same pace for all systems, the dissociation of hydrate and the evolution of methane at the seafloor is reduced and delayed temporally. For 550 m depth, one may notice the rapid increase (nearly two orders of magnitude) in V_{CH_4} at $t = 100 \text{ yr}$. This increase marks the arrival of free gas at the seafloor, at which point the flux transitions from

aqueous methane to primarily gaseous methane. For the systems at 600 m and 700 m, this transition does not arrive within the 300 yr timescale of the plots, and in fact, for 700 m, gas does not appear at the seafloor at anytime within the first 1000 yr.

For the case of more moderate warming, $\Delta T = +3$ °C/100 yr (Figure 5, bottom), the distinction between the potentially unstable “shallow” region and the more stable “deep” region becomes more pronounced. Cumulative release profiles appear quite similar for systems at 350 m and 400 m depths, with only slightly reduced fluxes and a delay of about 20 yr in the appearance of significant methane at the seafloor for the 400 m case. Deeper cases exhibit notable reductions in V_{CH_4} . A system at 450 m depth evolves methane at the seafloor at $t = 100$ yr rather than $t = 60$ yr at the reduced ΔT , and the order-of-magnitude “surge” in V_{CH_4} due to the appearance of gas at the seafloor does not occur until $t = 180$ yr. Deeper systems now do not produce significant methane fluxes within the time period of interest. Also visible in the second panel is the lower flux for the 500 m vs. that at 550 m. Although the pressure is slightly higher at greater depths, increasing hydrate stability, it also results in high methane solubility, enhancing the transport of aqueous methane from the system during the initial stages of warming. Gaseous methane evolves out of the 500 m system around $t = 250$ yr, however, and this results in the rapid increases in V_{CH_4} for the 500 m case after that time. For $\Delta T = +5$ °C/100 yr, this effect is overwhelmed by the earlier evolution of significant gaseous methane in the 500 m case.

The expected ocean warming is not expected to be uniform at all locations and depths, as seen clearly in Figure 1. Shallower waters along the top of the continental shelves warm more than deeper waters down the continental slope. A more realistic estimate is to scale ΔT as a function of water depth, such that we can approximate the temperature regimes estimated by the coupled climate-ocean models. In Figure 6, we present two such scaled series of cumulative flux profiles vs. depth and ΔT . In the first panel, ΔT scales from $\Delta T = +5$ °C/100 yr at 350 m down to $+1$ °C/100 yr at 700 m and below, approximating the temperature excursion profile for a Barents Sea shelf locale. In the second panel, the variation is shallower, ranging from $\Delta T = +3$ °C/100 yr at 350 m down to $+1$ °C/100 yr at 600 m (with 700 m and

below showing no short-time temperature variation), more representative of the profile along the narrower Beaufort shelf.

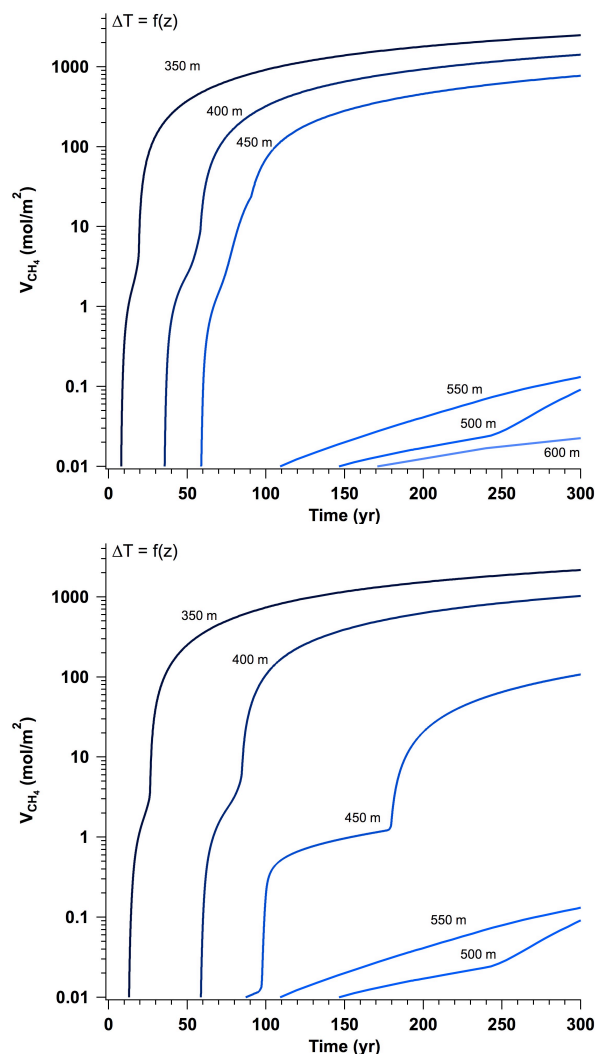


Figure 6. Cumulative local fluxes of methane in gaseous and aqueous phases, V_{CH_4} , at the seafloor for the warm (top) and cold (bottom) scenarios, with ΔT varying with depth. Note the log scale.

The top panel, the warm case, shows the strong separation between the “active” system—at water depths shallower than 500 m—and the deeper, less active systems with cumulative fluxes 2 to 3 orders of magnitude smaller. Similar to what is seen in the constant- ΔT evaluations, cumulative fluxes range from $V_{CH_4} = 30 - 1000$ mol/m² after 100 yr of warming within the active zone, but drop below 0.1 mol/m² for deeper locations. At $t = 300$ yr, shallower locations may contribute 500 – 2500 mol/m² without significant additional methane from deeper locations. In the lower panel, the cold

case, the shallower variation in ΔT leads to a less dramatic segregation between the active and less-active zones, but it is clear that only the shallowest—350 m and 400 m—cases contribute greatly to any large-scale methane release. The 450 m case shows that gas evolution is withheld until after $t = 180$ yr, and all deeper systems exhibit only small, aqueous releases of methane. Continued warming over a longer period would be expected to lower the top of the GHSZ and dissociate these hydrates over longer time scales.

It is clear that the most sensitive hydrate deposits under ocean temperature change scenarios will be located in a relatively narrow zone along continental margins, confined to regions where a combination of a strong warming signal and nearness to the edge of the GHSZ (a function of depth and initial temperature) leads to a plausible mechanism for rapid dissociation.

Integration of fluxes and regional estimates.

The goal of this extended research project is to assess, quantitatively, the possible global consequences of the injection of hydrate-derived methane into the oceans and atmosphere due to expected changes in ocean temperature. In previously published research [15,16], coupled ocean transport/methane biochemistry simulations establish that, under the conditions of hydrate-derived methane release, a considerable amount of methane could remain within the water column above and downcurrent from the release site as a consequence of resource limitations—most notably, the lack of sufficient oxygen to feed the biological conversion of methane to CO_2 . Such oxygen limitations both increase the potential for methane release into the atmosphere (important in that methane is a powerful greenhouse gas) and pose a heretofore-unanticipated biochemical impact on the ocean biosphere.

The simulation work by Elliott et al. [15,16] demonstrates that poorly ventilated basins, such as the sea of Okhotsk, could be severely impacted by the injection of 5.9×10^{12} mol CH_4 over a 30 yr period. Regions with more available oxygen, such as the Arctic Ocean, are more resilient to such releases, but significant methane plumes may form and persist, subjecting the local biological community to elevated methane concentrations and decreased oxygen concentrations. From the edge of the Beaufort basin (north of Point Barrow)

to the Queen Elizabeth Rise, approximately $1.1 \times 10^{11} \text{ m}^2$ of seafloor lies within the “active” zone for hydrate dissociation (350 m – 700 m). Taking bathymetry data from the NOAA ETOP2 dataset [31], we can divide the seafloor into 2 min blocks and bin those blocks at 50 m intervals to calculate the areal extent of seafloor at depth intervals from 350 m down to 700 m. Using the cold-scenario release curves from Figure 6, we can then estimate the total potential methane flux from each depth interval (estimating T and ΔT vs. depth as in the previous section) and sum these fluxes to compute the magnitude of hydrate-derived methane release within the zone of hydrate instability. Assuming ubiquitous but sparse hydrate within the GHSZ may be overly optimistic and direct observation of shelf hydrates in the Beaufort has been limited, but we can use this assumption as first estimate. This then leads to basin-wide cumulative release of $V_{\text{CH}_4} = 4.0 \times 10^{12}$ mol CH_4 at +30 yr after the appearance of gas at the seafloor for the cold scenario. This estimate is much like the assumed net source term for the coupled ocean transport/biochemistry studies [16], which injected a total of 3.9×10^{12} mol CH_4 over a 30 yr period into the Beaufort basin (localized, however, at two points, one near Barrow and one on the Queen Elizabeth Rise). In the case of the warm scenario, the larger local fluxes integrate to $V_{\text{CH}_4} = 6.0 \times 10^{12}$ mol CH_4 at +30 yr, very similar in magnitude to the assumed release.

Such injections resulted in localized methane plumes and corresponding localized reductions in dissolved oxygen [16], although for the well-ventilated Arctic Ocean waters, this alone is not enough to shut down methanotroph activity. However, a similar release in a poorly ventilated basin such as the Bering shelf or the Sea of Okhotsk would have far more dramatic consequences, with ocean chemistry simulations suggesting rapid progress toward hypoxia and widespread transport of dissolved methane [16]. Also, widespread increases in methane flux along the entire Arctic Ocean rim could eventually overwhelm the ability of the ecosystem to utilize the methane [15]. As a result, continued analysis of the possibility of hydrate destabilization is warranted, with a particular focus on refining physics-based numerical estimates of dissociation and coupling these estimates to the best available ocean chemistry and circulation models.

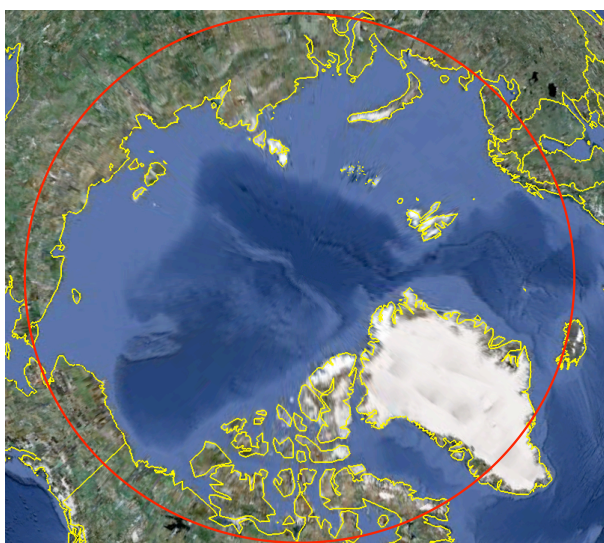


Figure 7. Extent of bathymetric integration for the Arctic basin-scale assessment. The red line approximates the 66°N north parallel. (Google Earth image)

Arctic Ocean assessment. The integration technique described above can be extended to a basin-scale assessment that encompasses the entire Arctic Ocean. To do this, we take a 4-minute subsample of the ETOPO2 bathymetric grid [31] for all seafloor north of 66°N latitude (Figure 7). Once again, we compute the total areal extent of every 50 m depth interval from 350 m down to 700 m. We then multiply the cumulative methane flux curves by the areal extent of their depth interval, and produce cumulative flux curves for each depth across all of the Arctic Ocean basin. The summation of these curves will then be an estimate of the total methane released into Arctic Ocean waters.

Figure 8 shows the evolution of $V_{\text{CH}_4, \text{tot}}$ for the warm scenario (ΔT ranging from 5 °C/100 yr to 1 °C/100 yr, varying with depth). The cumulative fluxes from Figure 6 have been multiplied by the areal extent of their respective depth range, and the plot shows the relative contribution of each depth range to the total methane release. The dashed red line indicates the total release of methane into Arctic water for all shallow hydrates north of the 66°N parallel. As the data is presented in log-linear form, it is clear that the shallowest (most sensitive to temperature change, and most productive) contribute by far the greatest proportion of the methane. As seen in the early simulation study, cumulative release decreases with both decreasing

ΔT and increasing depth, thus segregating a large proportion of shallow hydrates from the “bathtub ring” of potential release. This integration gives a methane release of 0.16×10^{15} mol CH_4 at +30 yr after the appearance of gaseous methane ($t = 50$ yr in simulation time), 0.66×10^{15} mol CH_4 at +100 yr ($t = 120$ yr), and 1.8×10^{15} mol CH_4 after +300 yr ($t = 320$ yr).

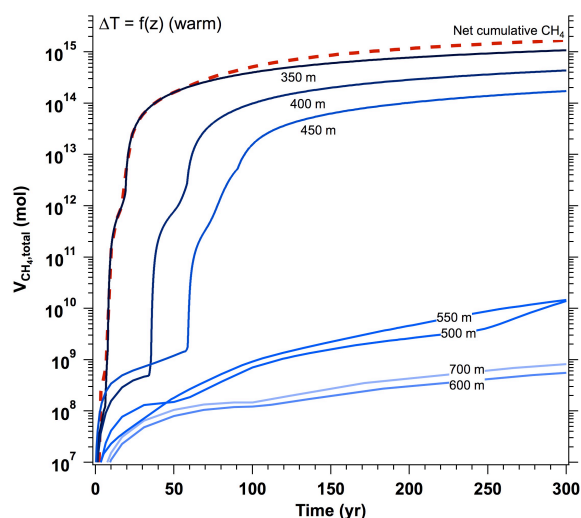


Figure 8. Cumulative local fluxes of methane in gaseous and aqueous phases, $V_{\text{CH}_4, \text{tot}}$, for a warm scenario ($\Delta T = 1$ °C - 5 °C/100 yr), plus the total basin-wide net flux (red line).

Figure 9 shows the evolution of $V_{\text{CH}_4, \text{tot}}$ for the cold scenario (ΔT ranging from 3 °C/100 yr to 0 °C/100 yr, varying with depth). As in the example of local cumulative release (Figure 6), the cold configuration shows a less dramatic separation between the active and inactive depth ranges, but still orders-of-magnitude differences across the depth range. This integration gives a methane release of 0.13×10^{15} mol CH_4 at +30 yr after the appearance of gaseous methane ($t = 55$ yr in simulation time), 0.49×10^{15} mol CH_4 at +100 yr ($t = 125$ yr), and 1.4×10^{15} mol CH_4 after +300 yr ($t = 325$ yr).

The total, basin-wide releases are replotted on a simpler linear scale in Figure 10, for direct comparison. To get a sense of the range of methane range values, we also plot the result of two uniform temperature integrations, where $\Delta T = +1$ °C or $\Delta T = +5$ °C at all depths while all other simulation and integration methodologies are performed as in the other cases. The small increase in the total released methane for the $\Delta T = +5$ °C

vs. the warm scenario once again indicates that the shallowest and most warming-sensitive hydrates contribute by far the most methane. The conservative $\Delta T = +1^\circ\text{C}$ scenario sets a lower bound, which, in comparison to the earlier scenarios, releases 0.11×10^{15} mol CH_4 at +30 yr after the appearance of gaseous methane ($t = 90$ yr in simulation time), 0.31×10^{15} mol CH_4 at +100 yr ($t = 160$ yr), and would release 0.72×10^{15} mol CH_4 after +300 yr ($t = 360$ yr).

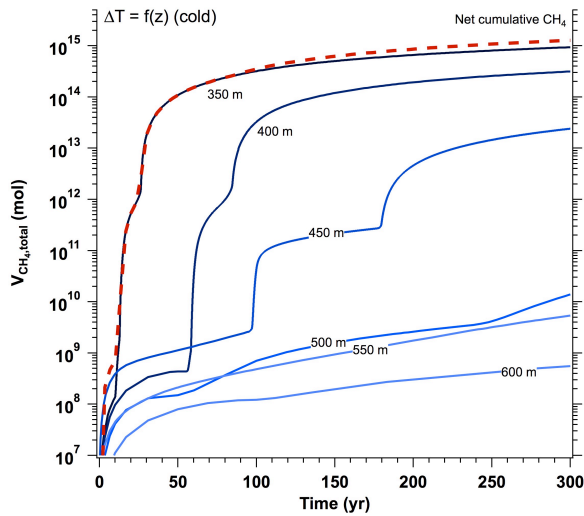


Figure 9. Cumulative local fluxes of methane in gaseous and aqueous phases, $V_{\text{CH}_4,\text{tot}}$, for a cold scenario ($\Delta T = 0^\circ\text{C} - 3^\circ\text{C}/100$ yr), plus the total basin-wide net flux (red line).

In comparison, the previous coupled methane biochemistry and ocean circulation simulations assumed that the six localized releases would add 10.8×10^{12} mol CH_4 to the Arctic Ocean basin after 30 yr of gaseous release, and nearly 36×10^{12} mol CH_4 after 100 yr [16]. The methane release described here is several orders of magnitude larger, suggesting that the biogeochemical effects noticed for the lower fluxes are certainly important to consider for these much larger releases. In addition, as the methane fluxes increase, resource limitations are expected to impact the ability of methanotrophs to consume the methane, resulting in the increased possibility of methane release to the atmosphere.

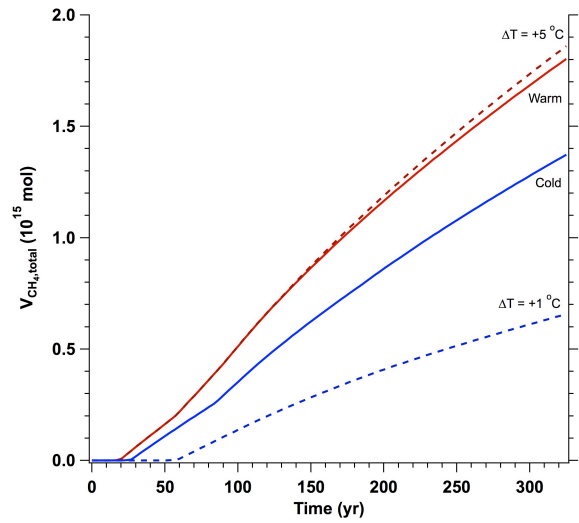


Figure 10. Cumulative basin-wide net release of methane in gaseous and aqueous phases, $V_{\text{CH}_4,\text{tot}}$, for the cold and warm scenarios, as well as $\Delta T = +1^\circ\text{C}$ and $\Delta T = +5^\circ\text{C}$ uniform warming at all depths. Note the linear scale.

CONCLUSIONS

A basin-scale assessment of submarine hydrates along the Arctic Ocean continental slope reveals a new, limited view of the possibility of a “clathrate gun” methane release event and its potential impact on the Arctic Ocean environment.

- 1) Sparse hydrates alone can release significant quantities of methane under the influence of moderate changes in the overlying water temperature. The release is controlled rather than explosive, due to the moderating influence of heat transfer through sediments, the endothermic nature of hydrate dissociation, and the limitations of gas transfer through marine sediments.
- 2) The release of methane at the seafloor due to warming of the overlying ocean is a function of initial temperature, depth of the water column above the hydrate-bearing sediments, and the magnitude and rate of temperature change.
- 3) These competing effects suggest that release of hydrate-derived methane due to ocean warming is likely to occur along a narrow “active” zone, beginning at the top of the GHSZ for a given water-column temperature regime and extending

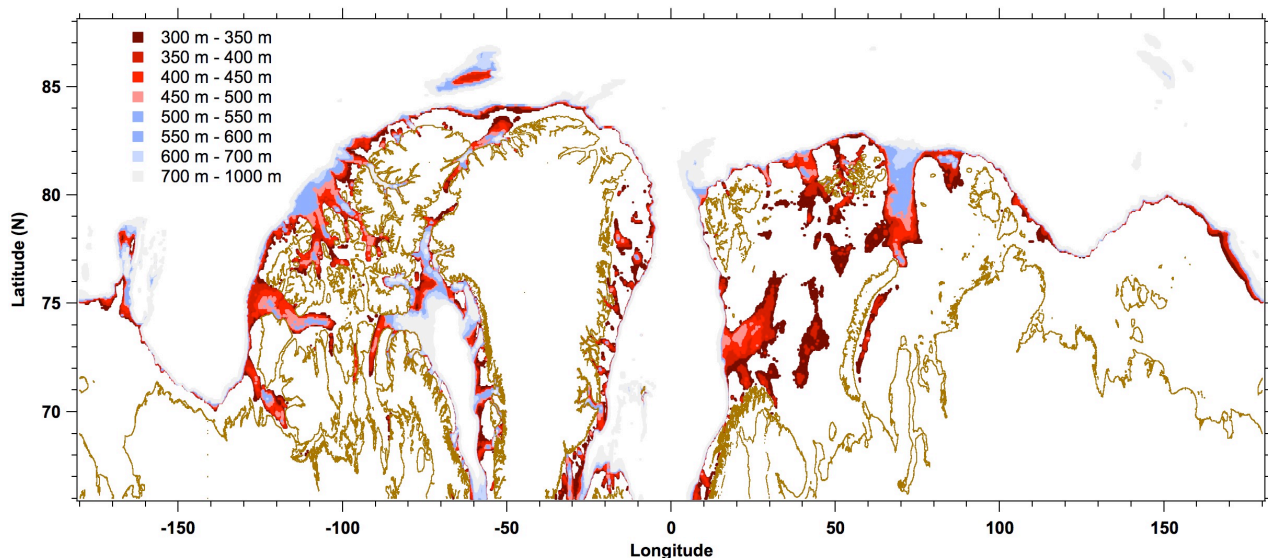


Figure 11: Depth contours [31] for the regions of the Arctic Ocean seafloor within the “bathtub ring” of hydrates sensitivity. Red zones are the regions of high potential release (< 500 m), blue zones are the regions of low potential release (> 500 m) for the warming scenarios described above. Coastlines [36] appear as beige lines, and only regions above 66°N latitude are shown. The vertical scale stretched for print legibility, and note that areal distortion is greater at high latitudes due to the x-y projection.

to the depth where increasing water pressure results in hydrate that is stable under the influence of expected temperature changes. This region is likely to occur only from the shallowest possible extent of the GHSZ (slightly deeper than 300 m under the coldest conditions) to about 500 m, at which depth rapidly moves the deposit deeper into the stability zone, reducing temperature sensitivity, potential temperature changes, and short-term release potential dramatically. Figure 11 plots the extent of this “bathtub ring” of sensitivity on a simple x-y projection of the globe north of 66°N latitude [36]. Depths prone to significant destabilization are contoured in red tones, those prone to less destabilization are contoured in blue-gray tones. Note the relative thinness of the sensitive region in areas such as the northern margin of Russia, the Beaufort Sea, and the broader regions of potential sensitivity along the Canadian Archipelago, and the Barents Sea. The widespread thinness of this zone of sensitivity limits the areal extent of potentially unstable hydrates, and limits the potential flux of methane that could be generated by short-term warming.

4) The vast stores of hydrate methane in the deep ocean are likely to be stable for all expected climate-change scenarios.

5) Regional estimates of hydrate dissociation and methane release currently match the magnitude of release assumed in previous coupled ocean biochemistry/transport studies, suggesting that the observed consequences—methane plumes, hypoxia, pH reduction, and partial transfer of methane to the atmosphere—need to be considered and the magnitudes assessed. That these basin-scale estimates greatly exceed what has been studied previously heightens concerns about the biological consequences of hydrate dissociation. Nonreactive “tracer” methane release in teramol quantities has the ability to reach the atmosphere via the ocean surface [16], and although chemistry should mitigate this release, the potential for much larger releases must be considered. Even if the potential methane transfer to the atmosphere is too low to create significant climate feedbacks, these processes demand evaluation.

6) Basin-scale estimates over the entire Arctic basin give a range of 0.1 to 0.5×10^{15} mol CH_4 (1.6 to 8 Gton CH_4) that could be released into the water column in the century following the appearance of methane plumes, with an additional 0.55 to 1.35×10^{15} mol CH_4 (4.3 to 22 Gton CH_4) over the subsequent two centuries without any further temperature change.

REFERENCES

- [1] Sloan ED, Koh C. *Clathrate Hydrates of Natural Gases*, 3rd Edition. CRC Press, New York, NY, 2007.
- [2] Gornitz V, Fung I. *Potential distribution of methane hydrate in the world's oceans*, *Global Biogeochem. Cycles* 1994; 8: 335-347.
- [3] Kvenvolden KA. *Potential effects of gas hydrate on human welfare*, *Proc. Nat. Acad. Sci.* 1999; 96: 3420-3426.
- [4] Borowski WS. *A review of methane and gas hydrates in the dynamic, stratified system of the Blake Ridge region, offshore southeastern North America*. *Chem. Geology* 2004; 205: 311-346.
- [5] Milkov AV. *Global estimates of hydrate-bound gas in marine sediments: how much is really out there?* *Earth Science Reviews* 2004; 66: 183-197.
- [6] Klauda JB, Sandler, SI. *Global distribution of methane hydrate in ocean sediment*. *Energy and Fuels* 2005; 19: 459-470.
- [7] Buffett B, Archer D. *Global inventory of methane clathrate: Sensitivity to changes in environmental conditions*. *Earth Planetary Sci. Lett.* 2004; 227: 185-199.
- [8] Reagan MT, Moridis GJ. *Dynamic response of oceanic hydrate deposits to ocean temperature change*. *J. Geophys. Res.* 2008; 113: C12023, doi:10.1029/2008JC004938.
- [9] Reagan MT, Moridis GJ. *Oceanic gas hydrate instability and dissociation under climate change scenarios*. *Geophys. Res. Lett.* 2007; 34: L22709, doi: 10.1029/2007GL031671.
- [10] Westbrook GK, Thatcher KE, Rohling EJ, Piotrowski AM, Palike H, Osborne AH, Nisbet EG, Minshull TA, Lanoiselle M, James RH, Huhnerbach V, Green D, Fisher RE, Crocker AJ, Chabert A, Bolton C, Beszczynska-Möller A, Berndt C, Aquilina A. *Escape of methane gas from the seabed along the West Spitsbergen continental margin*. *Geophys. Res. Lett.* 2009; 36: L15608, doi: 10.1029/2009GL039191.
- [11] Reagan MT, Moridis GJ. *Large-Scale Simulation of Oceanic Gas Hydrate Dissociation in Response to Climate Change*. *Geophys. Res. Lett.* 2009; 36: L23612, doi:10.1029/2009GL041332.
- [12] Kennett JP, Cannariato KG, Hendy LL, Behl RJ. *Carbon isotopic evidence for methane hydrate instability during quaternary interstadials*. *Science* 2000; 288: 128-133.
- [13] Xu W, Lowell RP. *Effect of seafloor temperature and pressure variations on methane flux from a gas hydrate layer: Comparison between current and late Paleocene climate conditions*. *J. Geophys. Res.* 2001; 106(B11): 26413-26423.
- [14] Valentine DL, Blanton DC, Reeburgh WS, Kastner M. *Water column methane oxidation adjacent to an area of active hydrate dissociation, Eel River Basin*. *Geochim Cosmochim. Acta* 2001; 65(16): 2633-2640.
- [15] Elliott SM, Reagan MT, Moridis GJ, Cameron-Smith PJ. *Geochemistry of Clathrate-Derived Methane in Arctic Ocean Waters*. *Geophys. Res. Lett.* 2010; 37: L12607, doi:10.1029/2010GL043369.
- [16] Elliott SM, Maltrud M, Reagan MT, Moridis GJ, Cameron-Smith PJ. *Marine Methane Cycle Simulations for the Period of Early Global Warming*. *J. Geophysical Res. Biogeo.* 2011; 116: G01010.
- [17] Kessler JD, Valentine DL, Redmond MC, Du M, Chan EW, Mendes SD, Quiroz EW, Villanueva CJ, Shusta SS, Werra LM, Yvon-Lewis SA, Weber TC. *A Persistent Oxygen Anomaly Reveals the Fate of Spilled Methane in the Deep Gulf of Mexico*. *Science* 2011; doi: 10.1126/science.1199697.
- [18] Moridis GJ, Kowalsky MB, Pruess K. *TOUGH+HYDRATE v1.0 User's Manual: A Code for the Simulation of System Behavior in Hydrate-Bearing Geologic Media*. Report LBNL-0149E, Lawrence Berkeley National Laboratory, Berkeley, CA, 2008.
- [19] Moridis GJ. *Numerical Simulation Studies of Thermally-Induced Gas Production From Hydrate Accumulations With No Free Gas Zones at the Mallik Site, Mackenzie Delta, Canada*. SPE 77861, Proceedings, SPE 2002 Asia Pacific Oil and Gas Conference and Exhibition, Melbourne, Australia, October 8-10, 2002.
- [20] Moridis GJ, Reagan MT. *Strategies for Gas Production From Oceanic Class 3 Hydrate Accumulations*. OTC 18865, Proceedings, 2007 Offshore Technology Conference, Houston, Texas, USA, 30 April - 3 May 2007.
- [21] Moridis GJ, Reagan MT. *Gas Production From Oceanic Class 2 Hydrate Accumulations*. OTC 18866, Proceedings, 2007 Offshore Technology Conference, Houston, Texas, USA, 30 April - 3 May 2007.
- [22] Rutqvist J, Moridis GJ. *Numerical Studies of Geomechanical Stability of Hydrate-Bearing Sediments*. OTC 18860, Proceedings, 2007 Offshore Technology Conference, Houston, Texas, USA, 30 April - 3 May 2007.

- [23] Tang L-G, Li X-S, Feng Z-P, Li G., Fan S-S. *Control mechanisms for gas hydrate production by depressurization in different scale hydrate reservoirs*. *Energy & Fuels* 2007; 21: 227-233.
- [24] Moridis GJ, Sloan ED. *Gas production potential of disperse low-saturation hydrate accumulations in oceanic sediments*. *Energ. Convers. Manag.* 2007; 48: 1834-1849.
- [25] Archer D. *Methane hydrate stability and anthropogenic climate change*. *Biogeosciences* 2007; 4: 521-544.
- [26] Ginsburg GD, Soloviev VA. *Submarine Gas Hydrates*. St. Petersburg: 1998.
- [27] Spinelli GA, Giambalvo E, Fisher AT. *Sediment permeability, distribution, and influence on fluxes in oceanic basement*. *Hydrogeology of the Oceanic Lithosphere*, Cambridge University Press: E.E. Davis and H Elderfield, Eds., 2004.
- [28] Haake RR, Westbrook GK, Riley MS. *Controls on the formation and stability of gas hydrate-related bottom-simulating reflectors (BSRs): A case study from the west Svalbard continental slope*. *J. Geophys. Res.* 2008; 113: B05104, doi: 10.1029/2007JB005200.
- [29] Ludmann T, Wong HK. *Characteristics of gas hydrate occurrences associated with mud diapirism and gas escape structures in the northwestern Sea of Okhotsk*. *Marine Geology* 2003; 201: 269-286.
- [30] Meehl G, Stocker TF, Collins WD, and 12 others. *Global climate projections*, In: *Climate Change 2007: The Physical Basis*, In IPCC AR4, Cambridge University Press, 2007.
- [31] U.S. Department of Commerce, National Oceanic and Atmospheric Administration, National Geophysical Data Center, *2-minute Gridded Global Relief Data (ETOPO2v2)*, 2006.
- [32] Moridis GJ., Seol Y, Kneafsey T. *Studies of reaction kinetics of methane hydrate dissociation in porous media*, *Proceedings, 5th International Conference on Gas Hydrates*, Trondheim, Norway, 12-16 June 2005.
- [33] Van Genuchten MT. *A closed-form equation for predicting the hydraulic conductivity of unsaturated soils*, *Soil Sci. Soc.*, 1980; 44: 892-898.
- [34] Stone, HL. *Probability model for estimating three-phase relative permeability*, *Trans. SPE AIME*, 1970; 249: 214-218.
- [35] Soluri EA, Woodson VA. *1990 World Vector Shoreline*. *International Hydrographic Review*, 1990; LXVII(1).

ACKNOWLEDGMENTS

This research has been supported by the Assistant Secretary for Fossil Energy, Office of Natural Gas and Petroleum Technology, through the National Energy Technology Laboratory, and by the Director, Office of Science, Office of Biological and Environmental Research as part of the Climate and Earth System Modeling Program, under the U.S. Department of Energy Contract No. DE-AC02-05CH11231.